Regular paper

Heat shock protein 90α inhibitor, PU-H71 in combination with DHEA promoting apoptosis in triple-negative breast cancer cell line MDA-MB-231

Hadeer Soudan[1], Hesham Saeed[1✉], Maha Eldemellawy[2,3], Manal Shalaby[2], Mostafa Hassan[4], Mohamed Elkewedi[5] and Nefertiti El-Nikhely[1]

[1]Department of Biotechnology, Institute of Graduate Studies and Research, Alexandria University, Alexandria, Egypt; [2]Genetic Engineering and Biotechnology Research Institute (GEBRI), City for Scientific Research and Technology Applications, New Borg Al-Arab City, Alexandria, Egypt; [3]Center of Excellence for Drug Preclinical Studies, City for Scientific Research and Technology Applications, New Borg Al-Arab City, Alexandria, Egypt; [4]Department of Environmental Studies, Institute of Graduate Studies and Research, Alexandria University, Alexandria, Egypt; [5]Department of Medical Laboratory Technology, Faculty of Applied Health Sciences Technology, Pharos University in Alexandria, Alexandria, Egypt

Due to the lack of markers (ER, PR, and HER-2/Neu) for the molecular-targeted therapies triple-negative breast cancer (TNBC) is more challenging than other subtypes of breast cancer. Moreover, the conventional chemotherapeutic agents are still the mainstay of most therapeutic protocols and eventually turn into a refractory drug-resistance , hence, more efficient therapeutic regimens are urgently required. The present study aimed to elucidate the effects of PU-H71 combined with DHEA on triple-negative breast cancer cell line MDA-MB-231 and to assess the synergy using the Chou-Talalay method. The combined therapy controlled the expression of an array of antioxidants and metabolizing enzymes, leading to the induction of oxidative stress which in turn induced apoptotic cell death. Our results indicated that the combined treatment with PU-H71 and DHEA exerts a synergistic anti-tumor effect on MDA-MB-231 triple-negative breast cancer cell line.

INTRODUCTION

Breast cancer (BC) is a complex disease, the most frequently diagnosed cancer, and the most leading cause of death among females all over the world (Godone *et al.*, 2018; Bray *et al.*, 2018). According to the GLOBOCAN database, BC is the most frequent cause of death in women in less developed regions, and the second in more developed countries, but compared to other cancers it is more equally distributed across regions (Bray *et. al.*, 2018). Triple-negative breast cancer (TNBC) is one of the most biologically aggressive subtypes of breast tumors, very often lethal and represents 15–20% of all diagnosed BC cases (Pareja *et al.*, 2016; Fabbri *et al.*, 2020). TNBC is characterized by lack of the expression

of estrogen receptor (ER), progesterone receptor (PR) and human epidermal growth factor receptor-1 (HER-2; also known as ERBB2) and therefore is one of the most puzzling women tumors and appears to be a poor candidate for a standardized sufficiently active therapeutic strategy (Fabbri *et al.*, 2020; Diana *et al.*, 2018; Dai *et al.*, 2018; Dai *et al.*, 2015). TNBC shows an unfavorable prognosis due to the early relapse within about 1-3 years and metastasis to other organs initiating new tumors (Dai *et al.*, 2015). Although TNBC patients initially show a good response to the conventional chemotherapy, they suffer from a chemo-resistance after disease relapses and respond neither to hormonal therapy nor to anti-HER2 agents as they lack their targets which makes the treatment more challenging (Pareja *et al.*, 2016; Nakai *et al.*, 2018). TNBCs are characterized by fast proliferation, poor differentiation, histopathological heterogeneity and higher ambiguity at the molecular level. These characteristic features offer few recurrent actionable targets to the clinicians, moreover, they direct the future roadmap of therapeutic regimens toward the combination therapy, which achieves superior therapeutic outcomes in comparison to monotherapy (Fabbri *et al.*, 2020; Chalakur-Ramireddy & Pakala, 2018; Lu *et al.*, 2013). Heat shock proteins (HSPs) are a group of proteins (also known as molecular chaperones) that function in response to stress or high temperature to reverse or inhibit denaturation or unfolding of cellular proteins. Based on their molecular weights, HSPs are classified as Hsp27, HSP40, Hsp60, Hsp70, Hsp90 and large HSPs (Hsp110 and glucose-regulating protein 179, GRP170) (Wu *et al.*, 2017). Heat shock protein 90 (Hsp90) is one of the most conserved HSPs that act as a defense mechanism during stressful conditions since they are overexpressed to reverse or inhibit the denaturation of cellular proteins and guarantee their proper folding (Hoter *et al.*, 2018; Joshi *et al.*, 2018; Ikwegbue *et al.*, 2018). Cancer cells rely on the molecular chaperones to survive as well as to acquire and maintain their malignant phenotype through the proper folding of the client proteins responsible for these functions (Sidera & Patsavoudi, 2014). Molecular chaperones are thought to play significant roles in molecular mechanisms leading to cancer development and metastasis, therefore, inhibiting the function of Hsp90 is a promising therapeutic target, which exhibits a combinatorial effect *per se*. PU-H71 (8-[(6-iodo-1,3-benzodioxol-5-yl)sulfanyl]-9-[3-(propan-2-ylamino) propyl] purin-6-amine) is a synthetic, water-soluble, purine-based Hsp90 inhibitor that was de-

veloped by NCI and Chiosis and others (Caldas-Lopes *et al.*, 2009) at Memorial Sloan-Kettering Cancer Center. It selectively binds to ATP-binding site in the N-terminal domain (NTD) of Hsp90, blocking its chaperoning function, and resulting in degradation of the client proteins (Speranza *et al.*, 2018). Further studies revealed that it downregulates a group of clients including elements of the RAS/RAF/MAPK pathway, cell-cycle regulators, anti-apoptotic factors, and Serine Threonine Protein Kinase B (Akt) (Fulda *et al.*, 2010). It showed a potent anti-tumor effect in TNBCs mouse xenografts with doses well tolerated by the host (up to 75 mg/kg). This dose showed a complete and durable response in TNBCs xenografts suggesting that TNBCs could be treated using PU-H71 over several cycles during over five months without exhibiting host toxicity (Calda-Lopes *et al.*, 2009; Trendowski, 2015). Unfortunately, like for other targeted drugs, it was reported that the viability of PU-H71-treated MDA-MB-231 cells was rescued , and the cells acquired resistance via two mechanisms. First, by the development of single nucleotide polymorphism (SNP) in the locus encoding the NTD of the Hsp90, which in turn decreased the sensitivity to bind the inhibitors, but not ATP. Second, by overexpression of Hsp90, which would protect the malignant cells from the proteotoxic stress of the misfolded proteins and from the effect of Hsp90 inhibitors, regardless of any mutations modifying the structure and/or conformation of Hsp90 (Miller *et al.*, 2016). Therefore, including Hsp90 inhibitors like PU-H71 in combination therapy is assumed to be a good approach to avoid the development of resistance by simultaneous targeting of several pathways, especially with aggressive tumors like TNBCs.

Glucose-6-phosphate dehydrogenase (G6PD) is a housekeeping protein that is constitutively expressed in all cells and overexpressed in numerous types of cancers including breast cancer. It regulates the first rate-limiting step of the oxidative branch of the pentose phosphate pathway (PPP), the main source of the reduced nicotinamide adenine dinucleotide phosphate (NADPH) that is crucial to maintain the reduction and oxidation (redox) homeostasis and has a role in lipids biosynthesis as well (Nagashio *et al.*, 2019; Benito *et al.*, 2017; Cernaj, 2016; Cho *et al.*, 2018). Therefore, G6PD is one of the vital enzymes activated during oxidative stress to protect the cells from damage by reactive insults. Unlike normal cells, cancer cells are characterized by metabolic aberrations and activation of oncogenic signals that cause extensive accumulation of reactive oxygen species (ROS), so they are more vulnerable to oxidative damage and more dependent on their antioxidant mechanisms (Wang *et al.*, 2019; Trachootham *et al.*, 2009). Therefore, blocking G6PD activity would disrupt the G6PD-mediated redox homeostasis by decreasing the cellular antioxidant capacity and finally induce a state of oxidative stress, which causes preferential cancer cell death. Dehydroepiandrosterone (DHEA) is one of the circulating steroids in humans, which is endogenously secreted from adrenal cortex and gonads as a precursor for the synthesis of male and female sex hormones (Cho *et al.*, 2018). It is a non-competitive inhibitor of G6PD that shows anti-proliferative and anti-migratory effects against TNBCs both *in vitro* and *in vivo* when used at pharmacological doses (Cho *et al.*, 2018; Hakkak *et al.*, 2017; Di Monaco *et al.*, 1997; Lopez-Marure *et al.*, 2011; Coli-Val *et al.*, 2017). In addition, it overcame the acquired chemo-resistance against paclitaxel in TNBCs caused by increasing the cellular antioxidant capacity (Cho *et al.*, 2018). Knocking down G6PD rendered cancer cells more vulnerable

to oxidative stress induced by pro-oxidants. Likewise, experiments including genetic deletions in mouse embryonic stem cells revealed that G6PD was not vital for proliferation nor pentose phosphate synthesis, but it was a key defender against oxidative stress. Accordingly, the *in vitro* growth of cancer cells was marginally affected by knocking down G6PD alone without incorporating any exogenous oxidative insults (Sukhatme & Chan, 2012). Therefore, inhibitors of G6PD could be good candidates to be included in combination therapy targeting the cellular oxidative homeostasis.

MATERIALS AND METHODS

Chemicals and biologicals. Neutral red dye, dimethyl sulfoxide (DMSO) and 2',7'-dichlorofluorescein diacetate (H2DCFDA) (Cat. no. D6883) were purchased from Sigma-Aldrich (St. Louis, Missouri, USA). PU-H71 and DHEA were purchased from Bio-Vision Inc. (Milpitas, California, USA). Dulbecco's Modified Eagle Medium-High glucose with glutamine (DMEM) and Fetal Bovine Serum (FBS) were purchased from Biowest (Riverside, Missouri, USA). RNeasy Mini kit was purchased from Qiagen (Cat. no. 74104, Germany). AMV Reverse Transcriptase was purchased from Promega Inc (Cat. no. M5108). SensiFAST™ SYBR® NO-ROX kit was purchased from Bioline (Cat. no. BIO-98005). BD Pharmingen™ FITC Annexin V Apoptosis Detection Kit II was purchased from BD Biosciences (Cat. no. 556570).

Cell culture. MDA-MB-231 breast cancer cell line was purchased from the American Type Culture Collection (ATCC, Manassas, VA, USA). Cells were cultured in DMEM supplemented with 10% FBS, 100 U/mL penicillin and 100 mg/mL streptomycin and incubated in a humidified incubator containing 5% CO_2 at 37°C. The cells were passaged when they reached about 80–90% of confluency.

Experimental design of combinations analysis. The cytotoxic effect of different combinations was assessed to quantitatively determine their pharmacodynamics as synergism, additive effect or antagonism using CompuSyn software program (ComboSyn Inc., Para-mus, NJ. USA). Four concentrations of each drug were chosen; ($0.25 \times IC_{50}$, $0.5 \times IC_{50}$, $0.75 \times IC_{50}$ and IC_{50}) and the pharmacodynamics of all the possible binary combinations raised from these four concentrations was screened (16 combinations including 4 combinations based on constant ratio approach, for which the results were previously reported (Elwakeel *et al.*, 2019), and 12 combinations based on the non-constant ratio approach, which were assessed to reveal the optimum combination ratio to obtain the maximal synergistic effect).

Cytotoxicity assay for different combinations of the tested drugs. PU-H71 and DHEA were dissolved in DMSO to prepare 10 mM stock solutions then serial dilutions were made in a complete growth medium and these were used to prepare the different concentrations used in cytotoxicity experiments. Cytotoxicity of each drug against MDA-MB-231 cell line was assessed using the neutral red uptake assay. Then, the dose-effect curve of each drug alone was created using CompuSyn Software (Elwakeel *et al.*, 2019). In addition, using the same software, the following parameters were automatically determined for each drug alone: D_m which is the half-maximal inhibitory concentration of the drug (i.e. IC_{50}), r that represents the linear correlation coefficient of each dose-effect curve and m which describes the curve's shape (Chou & Martin, 2005; Chou, 2006). The cytotoxic effect of all combinations was

tested after 48 hours of incubation using the neutral red uptake assay (Repetto *et al.*, 2008). Briefly, MDA-MB-231 cells were seeded at a density of 4500–5000 cells/well and incubated at 37°C in a CO_2 incubator overnight. Cells were then treated with different concentrations of the tested drugs (six replicates per each concentration) and incubated for 48 hours at 37°C in a CO_2 incubator. After the incubation, drug solutions were discarded, the cells were washed twice with PBS (pH=7.4) and the neutral red medium was added (40 μg/mL) with subsequent incubation for two hours at 37°C in a CO_2 incubator. Then the cells were washed twice with PBS (pH=7.4) and the neutral red dye was extracted from the cells with the destaining solution (50% ethanol, 49% de-ionized water and 1% glacial acetic acid). The plates were vigorously shaken for 10 and the optical density (OD) was measured at 540 nm using a microplate reader (Spectro star, BMG Labtech). Then the % inhibition and the fraction affected (*fa*) for all used combinations were calculated using equation (1) and (2) respectively.

$$\% \text{ Inhibition} = 100 - \left[\frac{(\text{OD treated cells} - \text{OD media blank})}{(\text{OD vehicle control} - \text{OD media blank})} * 100 \right] \quad (1)$$

$$fa = \frac{\% \text{ Inhibition}}{100} \quad (2)$$

Where, "OD treated cells" was the mean of the absorbance readings of cells exposed to the used drugs; "OD vehicle control" was the mean of the absorbance readings of cells exposed to the maximum used concentration of the solvent compound (DMSO); and finally, "OD media blank'" was the mean of the absorbance readings of wells containing media without cells as the neutral red non-specific binding control.

$$^2(CI)_x = \frac{(D)_1}{(D_x)_1} + \frac{(D)_2}{(D_x)_2}$$

$$= \frac{(D)_1}{(D_m)_1 \left[\frac{fa}{(1-fa)} \right]^{\frac{1}{m_1}}} + \frac{(D)_2}{(D_m)_2 \left[\frac{fa}{(1-fa)} \right]^{\frac{1}{m_2}}} \quad (3)$$

Analysis of the pharmacodynamic interactions of the tested drug combinations. According to the Chou-Talalay method the combination index (CI) and the dose reduction index (DRI) for each combination have to be determined and both values were automatically calculated using the CompuSyn software. CI and DRI of each drug combination were calculated based on equations (3) and (5) (Chou, 2006), respectively.

Where: $(D_x)_1$ is the dose of the drug D_1 alone, which inhibits the growth of the cells by x%, $(D_x)_2$ is the dose of the drug D_2 alone, which inhibits the growth of the cells by x%, $(D)_1$ and $(D)_2$ are the doses of the drugs D_1 and D_2 in combination, which inhibit the growth of cells by x%. The $(D_x)_1$ and $(D_x)_2$ values can be easily calculated by rearranging the Median-Effect Equation (4) as follows:

$$D = Dm \left[\frac{fa}{(1-fa)} \right]^{\frac{1}{m}} \quad (4)$$

$$(DRI)_1 = \frac{(D_x)_1}{D_1}, (DRI)_2 = \frac{(D_x)_2}{D_2}, \quad (5)$$

Where: DRI>1 represents favorable dose reduction, while DRI<1 indicates unfavorable conditions and finally DRI=1 indicates no dose reduction.

Morphological changes. MDA-MB-231 cells were seeded at a density of 1×10^6 cells / T-75 flask, then the flasks were incubated at 37°C in 5% CO_2 overnight. Next day, the flasks were treated with the indicated concentrations of each drug alone, the combinations and the vehicle control. After 48 hours of incubation, the cells were visualized and photographed using an inverted microscope (Olympus-IX70) at magnification X100 and X200 to observe the difference in the percentage confluency between the different treatments and at magnification X400 to examine the cellular morphological changes caused by each treatment (Rahman *et al.*, 2016).

Quantitative polymerase chain reaction, qPCR. Total RNA was isolated from the cells treated with PU-H71 and DHEA alone and in combination and with the control vehicle using RNeasy Mini Kit (Qiagen, Germany), with a DNase digestion step following the manufacturer's protocol. The elution step was performed using 50 μL nuclease-free water. The concentration, purity, and integrity of the isolated purified total RNA were determined using Nanodrop. One microgram of the prepared total RNA was reverse transcribed into the first strand cDNA using High-Capacity cDNA reverse transcription kit (ThermoFischer) using the random hexamer primers according to the manufacturer's instructions. Quantitative real-time PCR was carried out in triplicates using Maxima SYBR Green qPCR Master Mix (ThermoFischer). Primers used were as follows: Nrf2 forward: 5'-GTTTCTTCGGCTACGTTTCA-3'; reverse, 5'-TCAATGTCCTGTTGCATACC-3'; Caspase-3 forward, 5'-TTTTTCAGAGGGGATCGTTG-3'; reverse, 5' CGGCCTCCACTGGTATTTTA-3'; Caspase-8 forward: 5'- CCTGGGTGCGTCCACTTT-3'; reverse, 5'-CAAGGTTCAAGTGACCAACTCAAG-3'; Caspase-9 forward: 5'-GTGGACATTGGTTCTGGAGGAT-3'; reverse, 5'-CGCAACTTCTCACAGTCGATG-3'; Hsp90 forward: 5'-GTGAACCTATGGGTCGTGG-3'; reverse, 5'-GGGATATCCAATAAACTGAG-3'; CDK-1 forward: 5'-GTAGTAACACTCTGGTACAG-3'; reverse, 5'-CAATTTCTGAATCCCCATGG-3'; Ki-67 forward: 5'-GAGGTGTGCAGAAAATCCAAA-3'; reverse, 5'-CTGTCCCTATGACTTCTGGTTGT-3' and GAPDH forward; 5'-AGAAGGCTGGGGCTGATTTG-3', reverse 5'-AGGGGCCATCCACAGTCTTC-3'. Primers were added to the reaction mixture at a final concentration of 250 nM. The reaction was prepared in a final volume of 20 μL by mixing 5 μL of each cDNA sample (diluted 1:5), 12.5 μL of SYBR Green, 0.5 μL of each primer, and the final volume was adjusted through the addition of RNase/DNase-free water. The reaction conditions used were as follows: 10 min at 95°C for 1 cycle followed by 40 cycles of 15 s at 95°C, 30 s at 56°C (58°C for caspase 9 and 8), and 30 s at 72°C. The specificity of each primer pair was verified by the presence of a single melting curve peak. Results were analyzed for the relative expression of mRNA normalized against GAPDH as a house-keeping gene. Finally, the results were analyzed using the equation, $n=2^{-\Delta\Delta CT}$ where n represents the fold of induction or inhibition of genes under investigation.

Monitoring the accumulation of ROS. Intracellular accumulation of ROS was monitored using the fluorescent probe H2DCFDA. MDA-MB-231 cells were seeded onto sterile glass cover slips in 6 well plates at a density of 7×10^4 cells per cover slip and incubated overnight at 37°C. The next day, the cells were treated with the chosen drug combination or 0.25% DMSO for 1.5, 3, 5, 7 and 24 hours. After the incubation period, the cells were washed once with 1X PBS, then 10 μM of H2DCFDA

in incomplete medium was added and the incubation was continued for 30 minutes at 37°C in the dark. Finally, the cells were washed again with 1X PBS twice and examined under a confocal microscope at magnification X200 with fluorescent excitation at 488 nm and detection at 530 nm (Kim *et al.*, 2013; Ling *et al.*, 2011). A positive control was prepared by treating the cells with 0.1% (v/v) hydrogen peroxide (H_2O_2) for one hour. Finally, the fluorescence intensities were analyzed using ImageJ software.

Apoptosis detection. Apoptosis was analyzed using Annexin V-FITC apoptosis detection kit (Miltenyi Biotec). Cells were seeded at a density of 3.5×10^5 into T-25 flask and incubated overnight at 37°C in 5% CO_2. Next day, the cells were treated with the indicated drug doses or the vehicle control and after 48- and 72-hours incubation periods (to check the signal strength), floating cells, and the attached cells were collected by trypsinization and centrifuged at 2000 rpm for 5 minutes. The supernatants were decanted, and the cell pellets were washed twice with 1× PBS and once with 1X binding buffer and resuspended in 1 mL 1X binding buffer. One hundred microliters were then transferred to a clean tube and 5 μL of annexin V-FITC and 5 μL of PI were added and the tubes were incubated at room temperature for 15 minutes in the dark. Finally, 400 μL of 1X binding buffer was added and the stained cells were analyzed at the Flow Cytometry Service core facility at the Center of Excellence for Research in Regenerative Medicine and its Applications using BD FACS Calibur flow cytometer (BD FACSCalibur, BD Biosciences).

Statistical analysis. Statistical analysis was performed using GraphPad Prism 5 software (GraphPad Software, Inc .). Student's t test (two-tailed) was used to compare two groups. When more than two groups were compared, differences among the groups were assessed using one-way ANOVA (Analysis of Variance) with Tukey's post-hoc test for unpaired non-parametric variables. Outliers were identified using ROUT with Q=1%. Data were expressed as mean ± S.E.M. or ± S.D. from at least two independent experiments and two replicates.

RESULTS

Assessment of the pharmacodynamic interactions of combining PU-H71 and DHEA

To determine the nature of the interaction between PU-H71 and DHEA as synergism, additive effect, or antagonism, the dose-effect curves for PU-H71 and DHEA applied alone to MDA-MB-231 TNBC cell line were constructed using the CompuSyn Software. This step also generated the parameters (D_m), (m), and (r), which are prerequisite for the further analysis of the combinations. Previously, it was reported that the D_m values (i.e. IC_{50}) of PU-H71 and DHEA were about 155 nM and 250 μM, respectively (Elwakeel *et al.*, 2019). Then, to assess the pharmacodynamic interactions of PU-H71 and DHEA combined at different ratios, MDA-MB-231 cells were treated with equipotent constant ratio combinations (1:1) and non-constant ratio combinations (Supplementary File 1 at https://ojs.ptbioch.edu.pl/index.php/abp/). Moreover, to evaluate drug interactions between PU-H71 and DHEA in more detail, the CI values and the DRI values for each drug within each combination were automatically calculated (Supplementary File 2 at https://ojs.ptbioch.edu.pl/index.php/abp/). Earlier in-
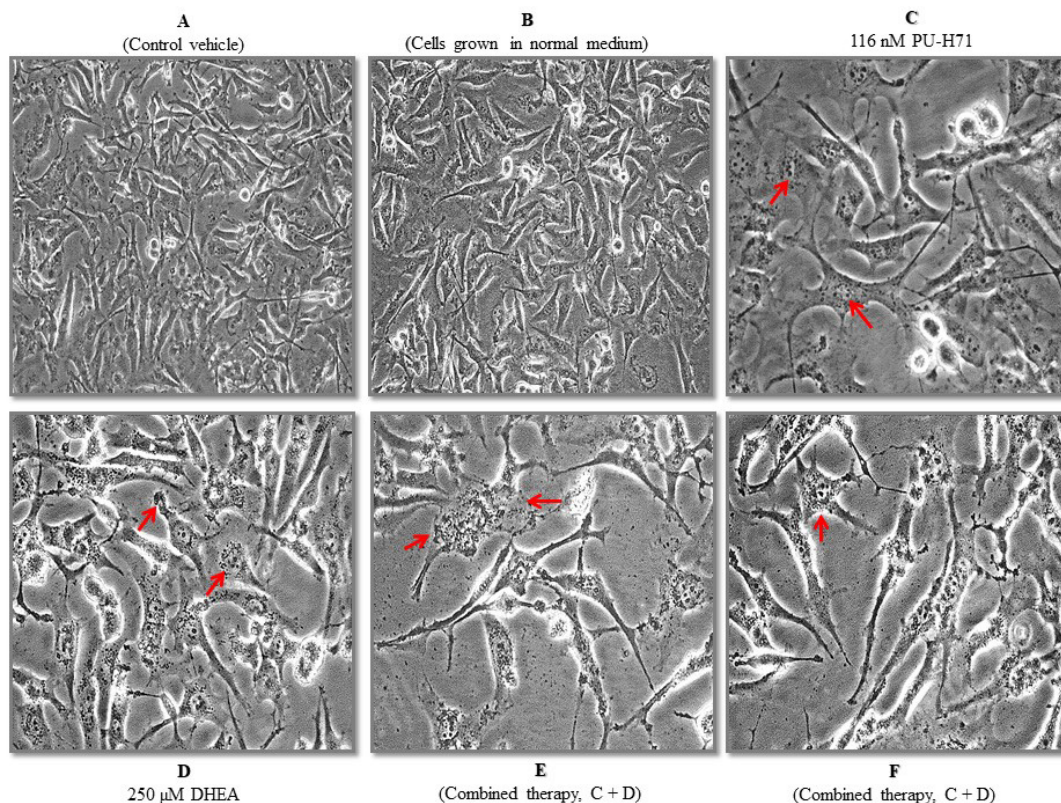

Figure 1. Light microscopy analysis of MDA-MB-231 TNBC cells morphology (magnification, X400) grown for 48 hours
(**A**) vehicle control cells, (**B**) cells grown in the normal growth medium, (**C**) cells treated with 116 nM PU-H71, (**D**) cells treated with 50 μM DHEA and (**E and F**) combined PU-H71/DHEA drugs-treated cells. Red arrows indicate cell shrinkage, membrane blebbing and detachment from the substratum.

vestigation showed that the combination of PU-H71 and DHEA at equipotent constant-ratio manner (1:1) resulted in synergistic effects proportional to the increasing concentration of both drugs (Elwakeel *et al.*, 2019). The non-constant combination ratios were also examined in order to find the optimum and two synergistic combinations were identified (Supplementary Files S2, S3 and S4 at https://ojs.ptbioch.edu.pl/index.php/abp/). Therefore, from the present experimental data points of all the tested combinations (including constant ratio and non-constant ratio), the optimum combination was chosen and it was the one which showed the highest *fa* (i.e. the highest % inhibition), the lowest CI value below 1 (i.e. the highest degree of synergism) and the highest DRI value especially for the most potent drug (PU-H71) (i.e. the lower expected toxicity). Therefore, the resulted optimal combination was 116 nM ($0.75 \times IC_{50}$) of PU-H71 with 250 μM (IC_{50}) of DHEA, where the cellular viability decreased by 83.13%, a moderate synergistic effect was present (CI=0.76) and the DRI value of DHEA was 1.34, while that of PU-H71 was 84.86. Although defining the pharmacodynamic effect of any combination is a crucial issue per se, this combination was chosen to be subsequently studied to, at least, overview some of the molecular events, underlying its mode of action.

Morphological changes

Morphological changes of MDA-MB-231 TNBC cells were examined after treatment with PU-H71 at a concentration of 116 nM, DHEA at 250 μM separately and in a combination for 48 h (Fig. 1A–F). It was observed that the confluency of cells was significantly reduced in a combination group compared to the other groups (Fig. 1E and F). Morphological changes were observed such as cells rounding and detachment from substratum, shrinkage, and reduction in size and membrane blebbing as compared to the control group (Fig. 1A and B) suggesting a decrease in the cell viability.

Analysis of gene expression of Hsp90, CDK-1, Ki-67, Nrf2, caspase 3, caspase 8 and caspase 9 by qPCR

The effect of PU-H71, DHEA alone and in combination on the expression levels of Hsp90 mRNA in MDA-MB-231 cells was studied and it was observed that the level of gene expression of the molecular chaperone Hsp90 was significantly up-regulated in PU-H71- and DHEA-treated cells by 8.6 and 2.7 folds, respectively, as compared to the control untreated cells (Fig. 2). Surprisingly, upon using a combination of PU-H71 and DHEA, the expression levels of Hsp90 were decreased as compared to the cells treated with either PU-H71 or DHEA alone but still significantly higher than in the control untreated cells by 3 folds (Fig. 2). To examine the effect of different treatments on the cell cycle and the proliferative potential of MDA-MB-231 cells, gene expression levels of cycle-dependent kinase-1 (CDK-1) and Ki-67 were determined. In cells subjected to the PU-H71/DHEA combined therapy the expression level of CDK-1 was decreased as compared to the PU-H71 treated cells (Fig. 2), while there was no significant change in CDK-1 mRNA level in comparison to the control ($p > 0.05$) and DHEA-treated cells ($p > 0.05$). The gene expression of Ki-67 was significantly upregulated (3 folds) in PU-H71 treated cells while a PU-H71/DHEA combined therapy resulted in highly significant downregulation of Ki-67 expression compared to PU-H71 treated cells (Fig. 2).

To examine the effect of the combined drug therapy on redox homeostasis of MDA-MB-231 cells, the lev-
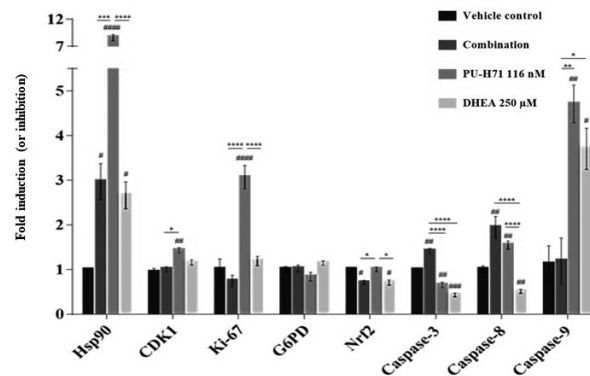

Figure 2. Quantification of the gene expression for the different treatments by qPCR.
The (#) symbol represents a significant difference compared to the vehicle control, while the (*) symbol represents a significant difference compared to the indicated groups. */#$p < 0.05$, **/##$p < 0.01$, ***/###$p < 0.001$ and ****/####$p < 0.0001$. The results are presented as the mean fold ± S.E.M. (n=3).

el of gene expression of Nrf2 was determined. It was observed that the expression of Nrf2 was significantly downregulated in cells subjected to the combined drug therapy compared to PU-H71-treated cells and the control group (0.7-fold) (Fig. 2). Moreover, the expression of Nrf2 was also downregulated in DHEA-treated cells when compared to the control cells (Fig. 2).

To investigate the effect of the selected drug combination on apoptosis, the level of gene expression of caspase 3, caspase 8 and caspase 9 was analyzed in all the tested groups. It was observed that the PU-H71-treated cells and the DHEA-treated cells showed a highly significant decrease of the expression levels of caspase-3 compared to the control cells by 0.66 and 0.43 fold, respectively (Fig. 2). On the other hand, the combined drug therapy exhibited a highly significant increase in the expression of caspase-3 in comparison to the control cells (1.4 fold), PU-H71 alone and DHEA alone. Regarding caspase-8, the combined therapy caused a significant upregulation of its expression when compared to the DHEA-treated cells and the control cells (1.7 fold), while there was no significant change in comparison to the PU-H71-treated cells ($p > 0.05$) (Fig. 2). In contrast, the combined therapy resulted in a significant downregulation of caspase-9 expression in comparison to the PU-H71 alone and DHEA alone, while both of them caused a significant increase in the expression of caspase 9 compared to the control cells by 4.7 and 3.7 fold, respectively.

Monitoring the intracellular accumulation of ROS

To further assess the effect of the selected drug combination therapy on the redox biology of MDA-MB-231 cells the intracellular accumulation of ROS after treatment with PU-H71, DHEA, PU-H71/DHEA combined drugs, 0.1% H_2O_2 (a positive control) and without treatment (normal complete growth medium) was assessed after 5 h for all the treatments except 0.1% H_2O_2, which was assessed after 1 h. The H2DCFDA staining of MDA-MB-231 cells revealed a high level of accumulated ROS in cells grown in the normal growth medium, vehicle control cells and cells treated with 0.1% H_2O_2 for 1 h as shown in Fig. 3A, B. On the other hand, MDA-MB-231 cells treated with either PU-H71 or DHEA alone, showed a highly significant decrease in the accu-
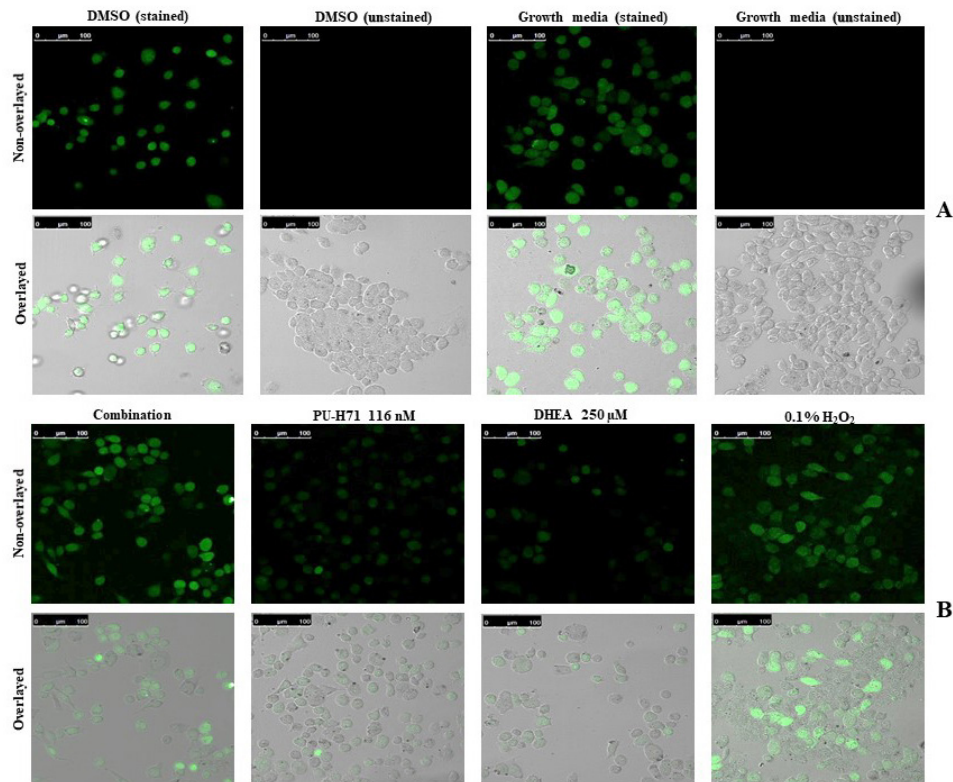
Figure 3. Confocal microscopy analysis (magnification X200) showing the accumulation of intracellular ROS in MDA-MB-231 TNBC cells grown in vehicle control medium and growth medium (A); cells treated with PU-H71/DHEA drugs combination, 116 nM PU-H71 alone, 250 μM DHEA alone and cells treated with 0.1% H_2O_2 (positive control).

mulation of ROS as compared to the control cells (Fig. 3B), while the cells treated with PU-H71 and DHEA combination showed a highly significant increase in ROS levels in comparison to all the other treatments (Fig. 3).

Apoptosis detection

To elucidate the apoptotic effects of PU-H71, DHEA alone and in combination, MDA-MB-231 cells were treated with the indicated drug concentrations and after the incubation period of 48 and 72 hours, the cells were double-stained with PI and annexin V-FITC and analyzed using a flow cytometer. The treatment for 48 hours showed no significant differences between none of the treatments neither in early apoptotic cells nor late apoptotic cells/dead cells. On the other hand, after increasing the incubation period to 72 hours the cells subjected to the combined therapy showed a significant increase in the population of the early apoptotic cells compared to the DHEA-treated cells ($p<0.05$), the PU-H71-treated cells ($p<0.001$) and the vehicle control cells ($p<0.0001$). Moreover, DHEA alone significantly increased the population of early ($p<0.001$) and late apoptotic cells ($p<0.05$), while PU-H71 alone caused a highly significant increase in early apoptotic cells only ($p<0.001$) compared to the vehicle control (Fig. 4A and B).

DISCUSSION

Triple-negative breast cancer is one of the most aggressive subtypes of BC that has the highest mortality rates and the worst prognosis (Shengling *et al.*, 2019). A better molecular characterization of TNBCs during the last decade has led to the development of new treatment strategies such as DNA damaging agents, poly-ADP-ribose polymerase inhibitors, androgen receptor blockade, and immunotherapy (Collingnon *et al.*, 2016; Bianchini *et al.*, 2016). Despite these advances, no targeted therapies have been approved for TNBCs. Therefore, it is of great importance to identify novel drugs that can effectively prevent and treat TNBC and have fewer side effects. Several signaling pathways and biomarkers were shown to be implicated in TNBC progression such as BAX/BCl2, Hsp90α, EGFR, VEGF, surviving, CDK-1, caspases, mTOR, and Ra/Raf/MEK/ERK (Sami *et al.*, 2020; Nedeljkovic & Damjanovic, 2019; Pellegrino *et al.*, 2020; Garrido-Castro *et al.*, 2019; Wang *et al.*, 209; Kordezngeneh *et al.*, 2015; Chatterjee & Burns, 2017; Su *et al.*, 2016). Many targeted therapies are currently combined based on the function of their targets or the evidence of additive or synergistic effects in a cell line (Su *et al.*, 2016). In this aspect, the focus of the current work was to investigate the therapeutic role of a combination of PU-H71/DHEA in MDA-MB-231 TNBC cell line. First, the cytotoxic effect of each drug alone was tested to generate the dose-effect curve of each drug and to determine D_m, m and r parameters as a prerequisite for drug combination analysis using CompuSyn Software. Then different combinations (Supplementary File 1 at https://ojs.ptbioch.edu.pl/index.php/abp/) were analyzed using the constant and non-constant ratio approach (Elwakeel *et al.*, 2019). Our results indicated that the combination with the highest synergistic effect was 116 nM of PU-H71 ($0.75 \times IC_{50}$) and 250 μM of DHEA (IC_{50}). This combination of PU-H71/DHEA drugs was found to decrease the viability of MDA-MB-231 cells by 83.13% with a moderate synergistic effect (CI=0.76) and the higher DRI value (i,e. for PU-H71) was 84.86 while
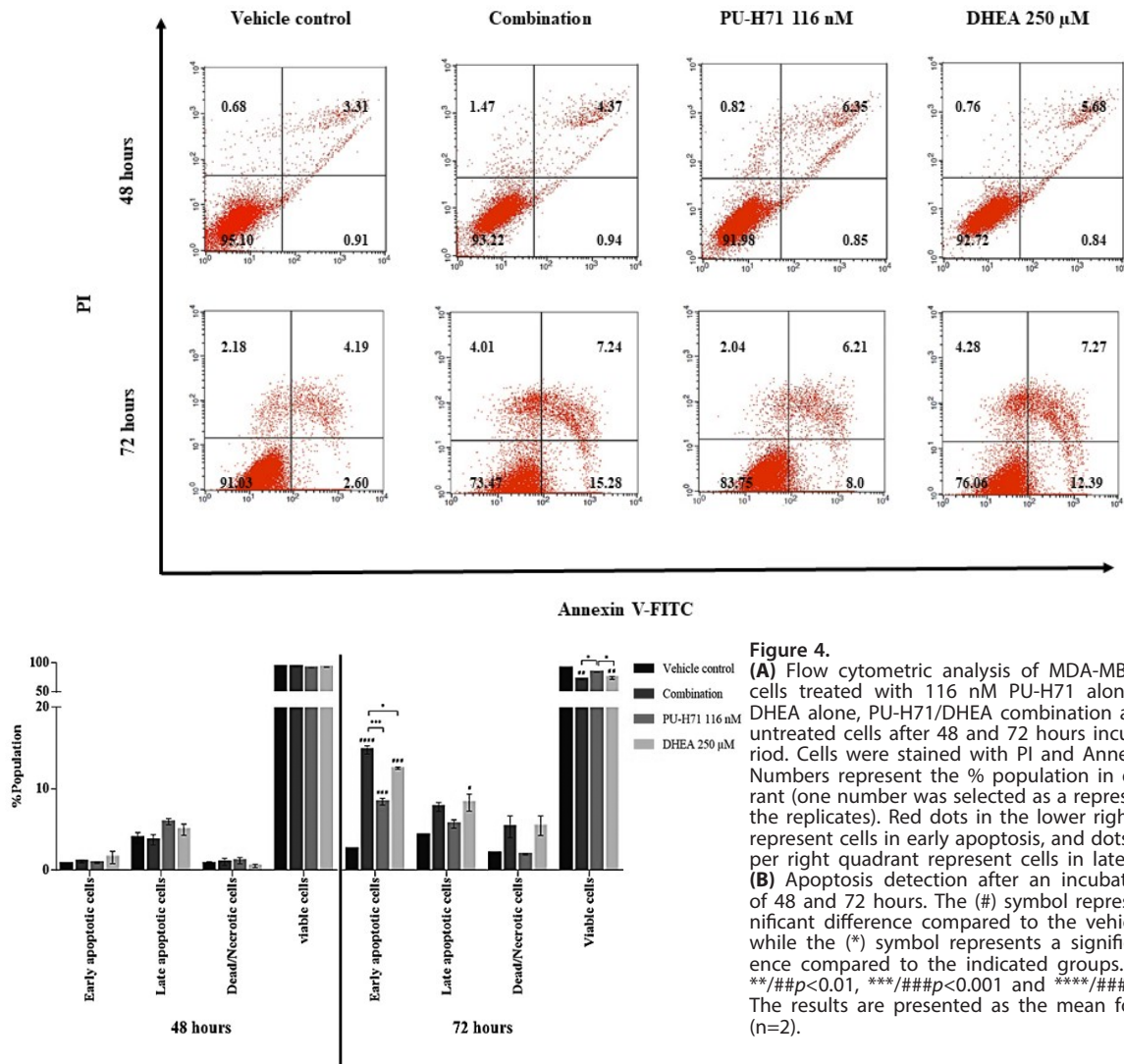
Figure 4.
(A) Flow cytometric analysis of MDA-MB-231 TNBC cells treated with 116 nM PU-H71 alone, 250 μM DHEA alone, PU-H71/DHEA combination and control untreated cells after 48 and 72 hours incubation period. Cells were stained with PI and Annexin V-FITC. Numbers represent the % population in each quadrant (one number was selected as a representative of the replicates). Red dots in the lower right quadrant represent cells in early apoptosis, and dots in the upper right quadrant represent cells in late apoptosis. **(B)** Apoptosis detection after an incubation period of 48 and 72 hours. The (#) symbol represents a significant difference compared to the vehicle control, while the (*) symbol represents a significant difference compared to the indicated groups. */#$p < 0.05$, **/##$p < 0.01$, ***/###$p < 0.001$ and ****/####$p < 0.0001$. The results are presented as the mean fold ±S.E.M. (n=2).

that of DHEA was 1.43. Moreover, this drug combination was subsequently investigated in detail to elucidate the molecular events by which it acted on TNBC cell line.

The upregulation of Hsp90 mRNA expression upon using a single drug, PU-H71 could be attributed to the development of a resistance mechanism by MDA-MB-231 cells (Rouhi *et al.*, 2017). Interestingly, the combined drug therapy, PU-H71/DHEA resulted in a significant reduction in Hsp90 expression suggesting a better therapeutic outcome in comparison to the single drug, PU-H71, although the level of Hsp90 gene expression was still higher than in the control cells. In TNBCs, Hsp90 forms a complex with regulatory proteins of the cell cycle including CDK-1 and checkpoint kinase 1 (ChK-1) which are crucial for Gap-2 (G2)-mitosis (M) progression. PU-H71 was found to trigger a decline in CDK-1 protein level in a dose-dependent manner and this was sufficient to delay the G2-M progression and subsequently stimulate the cell death of MDA-MB-231 cells (Calda-Lopes *et al.*, 2009). It causes downregulation of Hsp90 client proteins since inhibition of Hsp90 activity causes accumulation of the unfolded/miss-folded client proteins which are further degraded *via* the ubiquitin-proteasome system (Trendowski, 2015). Therefore, the significant increase in the mRNA level of CDK-1

in PU-H71-treated cells might not be necessarily a result of a higher level of the protein. In addition, our results revealed that there was no significant change in the expression level of CDK-1 in DHEA-treated cells compared to the control cells, so DHEA might not influence the cell cycle. It was previously reported that DHEA had no effect on the cell cycle of ER-negative cell lines including MDA-MB-231 cells treated with 100 μM of DHEA for 48 hours (Lopez-Marure *et al.*, 2011). Ki-67 is a proliferation marker located inside the nucleus in the course of interphase and during mitosis, and it is transferred to the chromosome's surface. It is present in the cells during the division phases of the cell cycle, Gap-1 (G1), synthesis (S1), G2 and M while it is absent during the resting phase, G0. It was reported that Ki-67 is overexpressed in ER-negative breast cancer cells and its expression in breast carcinoma cells was much higher than in normal tissue (Yadav *et al.*, 2015). CDK-1 is the key kinase which promotes entry into mitosis. Ki-67 is phosphorylated by CDK-1 during M phase, resulting in progression through mitosis (Menon *et al.*, 2019). Since both CDK-1 and Ki-67 were significantly downregulated in the combined therapy-subjected cells compared to PU-H71-treated cells, we suggested that DHEA might potentiate the effect of PU-H71 to decrease the proliferative potential of MDA-MB-231 cells and trigger cell

cycle arrest but, more studies at the protein level are still needed to confirm this finding. Nrf2 regulates the expression of different cytoprotective (detoxifying) genes and metabolic genes and hence it plays a vital role in cancer progression via modulating the cellular metabolism and maintaining the redox homeostasis (O'Loughlin et al., 2018). Therefore, the decrease in Nrf2 expression level (Fig. 2) would disrupt the redox homeostasis via declining the antioxidant capacity, resulting in oxidative damage of cancer cells and hence apoptotic cell death.

Apoptosis is an energy-consuming process involving activation of cysteine-aspartic proteases, caspases, which belong to two types: initiator caspases such as caspase 8 and 9 and the executioner or effector caspases like caspase 3 (Shengling et al., 2019; Collingnon et al., 2016). Caspase 8 is a key initiator caspase inducing apoptosis via the cell death receptor pathway (extrinsic pathway), while caspase 9 has a vital role in initiating apoptosis via the mitochondrial pathway (intrinsic pathway) (Bianchini et al., 2016). Our results showed that the combined PU-H71/DHEA drug therapy induced a highly significant increase in the expression of caspase 3 and caspase 8 compared to the control untreated cells, by 1.4 and 1.7 fold respectively, suggesting apoptosis induction via at least the extrinsic pathway. Thus, to verify the apoptosis induction flow cytometric analysis was carried out and it was observed that there were no significant differences between different treatment groups after 48 hours incubation period while after increasing the incubation period to 72 hours, the combined PU-H71/DHEA drug therapy-subjected cells showed a significant increase in the population of apoptotic cells compared to the control cells and each tested drug alone (Fig. 4A and B). Moreover, MDA-MB-231 cells treated with PU-H71 at a concentration of 116 nM alone for 72 hours displayed a highly significant increase in the early apoptotic cells (Fig. 4A and B). However, it was reported that PU-H71 induced apoptosis of the same cell line at 1 μM applied for 48 hours (Korkola et al., 2003). The mechanism by which PU-H71 induces apoptosis of TNBCs is attributed to Akt and B-cell lymphoma-extra-large (BCL-xl) proteins (Korkola et al., 2003). DHEA was reported to significantly increase the late apoptotic cells population of HeLa cells in a dose-dependent manner. This effect is due to the increased production of ROS inducing oxidative stress which in turn resulted in triggering apoptosis (Hotter et al., 2018). In this study, treating MDA-MB-231 cells with 250 μM DHEA for 48 hours did not induce apoptosis which is consistent with a previous study where treating the same cells with 100 μM of DHEA for 48 hours also did not result in apoptotic cell death (Nakai et al., 2018). However, our results revealed that treating MDA-MB-231 cells with DHEA at a concentration of 250 μM for 72 hours significantly increased the population of early and late apoptotic cells (Fig. 4A and B). Since caspases have a vital role in initiation as well as in the regulation of apoptosis, it could be suggested that the apoptosis induction in the PU-H71- and DHEA-treated cells might be at least via activation of the intrinsic apoptotic pathway since the expression level of caspase 9 was significantly increased compared to the control untreated cells (Fig. 2). However, the expression level of caspase 3 did not increase. While PU-H71 and DHEA drugs alone caused apoptotic cell death, their combination was still more effective because it targeted more than one pathway at the same time. The combination strategy decreases the chances of the resistance development that might be caused by using each drug alone, particularly during the treatment of the most aggressive and complicated cancers like TNBC.

Since it was postulated that the cells subjected to the combined therapy might suffer from oxidative stress, it was particularly interesting to investigate the difference in the level of the intracellular accumulated ROS level between the different treatments. We observed a persistent, high basal level of ROS in the control cells grown in the normal complete medium and the vehicle control (Fig. 3) which could be attributed to the high glucose concentration in the growth medium (25 mM) in which the MDA-MB-231 cells were sustainably cultured. It was previously reported that MDA-MB-231 cells grown in high-glucose medium (20 mM), showed high expression of Thioredoxin-Interacting Protein (TXNIP), which reduced the activity of thioredoxin (TXN) and hence increased the ROS level (Turturro et al., 2007). Moreover, the significant decrease in the ROS level in MDA-MB-231 cells treated with PU-H71 alone (Fig. 3) could be explained in analogy to a previous study that showed that Hsp90 inhibitors 17-AAG and 17-DMAG attenuated the oxidative stress via induction of some antioxidant enzymes such as manganese superoxide dismutase, glutathione peroxidase and catalase, which decrease the ROS level (Li et al., 2018). In addition, the NADPH oxidases (Nox), a family of seven enzymes, are the major source of ROS that consume NADPH to produce superoxide (Chen et al., 2011). Inhibition of Hsp90 caused destabilization of some of the Nox enzymes such as Nox 1, 2, 3 and 5, leading to a subsequent decrease in the production of superoxide since these Nox enzymes are considered Hsp90 client proteins. Regarding the DHEA-treated cells, a highly significant reduction of ROS level was observed (Fig. 3) and this observation was supported by a previous study, where DHEA reduced the death of muscle cells induced by H_2O_2 in a dose-dependent manner via induction of Nrf2 nuclear translocation and subsequent increase in the antioxidant capacity of the cells (Jeon et al., 2015). This finding is also in consistence with the results of a previous study in which DHEA acted as an antioxidant since it eliminated the high glucose-induced ROS and nitric oxide (NO) in the endothelial cells. DHEA also decreased the oxidative stress stimulated in rats by selenium and vitamin E deficiency in a dose-dependent manner (Huerta-Garcia et al., 2012). Consequently, 250 μM of DHEA was suggested to act as an antioxidant and decrease the basal ROS level during at least the first five hours of incubation with MDA-MB-231 that were chronically cultured under high-glucose condition. Finally, the cells subjected to the combined therapy showed a highly significant increase in the ROS level compared to the other treatments (Fig. 3). Under physiological conditions, Nrf2 is bound to Kelch-like ECH associated protein 1 (Keap-1) as it is ubiquitinylated and subsequently degraded via the proteasomal pathway. Under oxidative stress conditions, Keap-1 becomes unstable, while Nrf2 is stabilized, translocated to the nucleus and then binds to the oxidative response element (ARE) initiating the transcription of the cytoprotective genes (Mitsuishi et al., 2012). Consequently, if the level of Nrf2 is decreased, it reduces the cellular antioxidant capacity and aggravates the oxidative stress and its subsequent events. It could be expected that the tested combination therapy concurrently blocked the main presenters of the ROS-scavenging systems, the glutathione (GSH) and TXN systems. Decreasing the level of Nrf2 would reduce the pool of both GHS and TXN, whilst inhibiting the activity of Hsp90 would cause deg-

radation of TXN as TXN-1 is one of the Hsp90 client proteins (Kraika-Kuzniak et al., 2017).

Based on these finding, a possible molecular mechanism by which PU-H71/DHEA combined therapy-induced apoptosis could be hypothesized. Nrf2 was downregulated in the cells subjected to the combination therapy which induced oxidative stress *via* depletion of the cellular antioxidant capacity and hence the levels of ROS elevated above the cellular threshold level. Therefore, the combined drug therapy might induce apoptosis via the intrinsic pathway because of increasing the oxidative stress, although the level of gene expression of caspase 9 was significantly decreased. Moreover, the tested combination could induce apoptosis via the extrinsic pathway as elucidated by the significant upregulation of caspase 8 and caspase 3.

In conclusion, the pharmacodynamic assessment of combining PU-H71 as an Hsp90 inhibitor and DHEA as a G6PD inhibitor resulted in a synergistic effect against MDA-MB-231 TNBC cell line *via* the downregulation of Nrf2 which is a crucial transcription factor controlling the expression of an array of antioxidants and metabolizing enzymes. As a result, cellular antioxidant capacity was decreased leading to an increased level of intracellular ROS which exceeded the death threshold level and led to apoptotic cell death.

Conflict of interest

We declare that there is no conflict of interest regarding this article and there is no financial employment, consultancies, honoraria, stock ownership or options, expert testimony, royalties related to this manuscript. Moreover, we declare that this work has not been published elsewhere; have not been simultaneously submitted for publication elsewhere and all the authors have agreed to the submission.

REFERENCES

Benito A, Polat IH, Noé V, Giudad CJ, Marin S, Cascante M (2017) Glucose-6-phosphate dehydrogenase and transketolase modulate breast cancer cell metabolic reprogramming and correlate with poor patient outcome. *Oncotarget* **8**: 106693–106706. https://doi.org/10.18632/oncotarget.21601.

Bianchini G, Balko JM, Mayer IA, Sanders ME, Gianni L (2016) Triple-negative breast cancer: challenges and opportunities of a heterogenous disease. *Nat Rev Clin Oncol* **13**: 674–690. https://doi.org/10.1038/nrclinonc.2016.66.

Bray F, Ferlay J, Saerjomataram I, Siegel R, Torre LA, Jemal A (2018) Global Cancer Statistics 2018: GLOBOCAN estimates of incidence and mortality worldwide for 36 cancers in 185, countries. *CA A Cancer J Clin* **68**: 394–424. https://doi.org/10.3322/caac.21492.

Caldas-Lopes E, Cerchietti L, Ahn JH, Clement CC, Robles AI, et al. (2009) Hsp90 Inhibitor PU-H71, a multimodal inhibitor of malignancy, induces complete responses in triple-negative breast cancer models. *Proc Natl Acad Sci USA* **106**: 8368–8373. https://doi.org/10.1073/pnas.0903392106.

Cernaj IE (2016) Simultaneous dual targeting of Par-4 and G6PD: a promising new approach in cancer therapy? quintessence of a literature review on survival requirements of tumor cells. *Cancer Cell Int* **16**: 4–9. https://doi.org/10.1186/s12935-016-0363-9.

Chalakur-Ramireddy NKR, Pakala SB (2018) Combined drug therapeutic strategies for the effective treatment of triple-negative breast cancer. *Biosci Rep* **38**: BSR 20171357. https://doi.org/10.1042/BSR20171357.

Chatterjee S, Burns TF (2017) Targetting heat shock proteins in cancer: A promising therapeutic approach. *Int J Mol Sci* **18**: 1978. https://doi.org/10.3390/ijms18091978.

Chen F, Pandey D, Chadli A, Catravas JD, Chen T, Fulton DJR (2011) Hsp90 Regulates NADPH oxidase activity and is necessary for superoxide but not hydrogen peroxide production. *Antioxid Redox Signal* **14**: 2107–2119. https://doi.org/10.1089/ars.2010.3669.

Cho ES, Cha YH, Kim HS, Kim NH, Yook JI (2018) The pentose phosphate pathway as a potential target for cancer therapy.

Biomol Ther (Seoul) **26**: 29–38. https://doi.org/10.4062/biomolther.2017.179.

Chou TC (2006) Theoretical basis, experimental design, and computerized simulation of synergism and antagonism in drug combination studies. *Pharmacol Rev* **58**: 621–681. https://doi.org/10.1124/pr.58.3.10.

Chou TC, Martin N (2005) CompuSyn for Drug Combinations. *Paramus NJ*; 2005. http://www.combosyn.com.

Colín-Val Z, González-Puertos VY, Mendoza-Milla C, Gomez EO, Huesca-Gomez C, Lopez-Marure C (2017) DHEA increases epithelial markers and decreases mesenchymal proteins in breast cancer cells and reduces xenograft growth. *Toxicol Appl Pharmacol* **333**: 26–34. https://doi.org/10.1016/j.taap.2017.08.002.

Collingnon J, Lousberg L, Schroeder H, Jerusalem G (2016) Triple negative breast cancer: treatment challenges and solutions. *Breast Cancer Targets Ther* **8**: 93–107. https://doi.org/10.2147/BCTT.

Dai X, Li T, Bai Z, Yang Y, Liu X, et al. (2015) Breast cancer intrinsic subtype classification, clinical use and future trends. *Am J Cancer Res* **5**: 2929–2943. PMID: 26693050; PMCID: PMC4656721.

Di Monaco M, Pizzini A, Gatto V, Leonardi L, Gallo M, et al. (1997) Role of glucose-6-phosphate dehydrogenase inhibition in the antiproliferative effects of dehydroepiandrosterone on human breast cancer cells. *Br J Cancer* **75**: 589–592. https://doi.org/10.1038/bjc, doi: 10.1038/bjc.1997.102.

Diana A, Franzese E, Centonze S, Carlino F, Ventriglia J, et al. (2018) Triple-negative breast cancers: systematic review of the literature on molecular and clinical features with a focus on treatment with innovative drugs. *Curr Oncol Rep* **20**: 76. https://doi.org/10.1007/s11912-018-0726-6.

Elwakeel A, Soudan H, Eldoksh A, Shalaby M, Eldemellawy M, Ghareb D, Abouseif M, Fayad A, Hassan M, Saeed H (2019) Implementation of the Chou-Talalay method for studying the *in vitro* pharmacodynamic interactions of binary and ternary drug combinations on MDA-MB-231 triple negative breast cancer cells. *Synergy* **8**: 100047. https://doi.org/10.1016/j.synres.2019.100047.

Fabbri F, Salvi S, Bravaccini S (2020) Know your enemy: genetics, aging, exposomic and inflammation in the war against triple negative breast cancer. *Semin Cancer Biol* **60**: 285–293. https://doi.org/10.1016/j.semcancer.2019.10.015.

Fu S, Chen X, Lo H-W, Lin J (2019) Combined bazedoxifene and paclitaxel treatments inhibit cell viability, cell migration, colony formation, and tumour growth and induce apoptosis in breast cancer. *Cancer Lett* **448**: 11–19. https://doi.org/10.1016/j.canlet.2019.01.026.

Fulda S, Galluzzi L, Kroemer G (2010) Targeting mitochondria for cancer therapy. *Nat Rev Drug discov* **9**: 447–464. https://doi.org/10.1038/nchembio.1712.

Garrido-Castro AC, Lin Nu, Polyak K (2019) Insights into molecular classifications of triple negative breast cancer: improving patient selection for treatment. *Cancer Discov* **9**: 176–198. https://doi.org/10.1158/2159-8290.

Godone RLN, Leitão GM, Araûjo NB, Castelletti CHM, Lima-Filho JL, Martins DBG (2018) Clinical and molecular aspects of breast cancer: targets and therapies. *Biomed Pharmacother* **106**: 14–34. https://doi.org/10.1016/j.biopha.2018.06.066.

Hakkak R, Bell A, Korourian S (2017) Dehydroepiandrosterone (DHEA) feeding protects liver steatosis in obese breast cancer rat model. *Sci Pharm* **85**: 13. https://doi.org/10.3390/scipharm85010013.

Hoter A, El-Sabban ME, Naim HY (2018) The HSP90 family: structure, regulation, function, and implications in health and disease. *Int J Mol Sci* **19**: 2560. https://doi.org/10.3390/ijms19092560.

Huerta-García E, Ventura-Gallegos JL, Victoriano MEC, Victoriano MEC, Montiél-Dávalos Ikwegbue PC, Masamba P, Oyinloye BE, Kappo AB (2018) Roles of heat shock proteins in apoptosis, oxidative stress, human inflammatory diseases, and cancer. *Pharmaceuticals* (Basel) **11**: 1–18. https://doi.org/10.3390/ph11010002.

Huerta-García E, Ventura-Gallegos JL, Victoriano MEC, et al. (2012) Dehydroepiandrosterone inhibits the activation and dysfunction of endothelial cells induced by high glucose concentration. *Steroids* **77**: 233–240. https://doi.org/10.1016/j.steroids.2011.11.010.

Jeon S, Hur J, Kim J (2015) DHEA alleviates oxidative stress of muscle cells *via* activation of Nrf2 pathway. *App Biochem Biotechnol* **176**: 22–32. https://doi.org/10.1007/s12010-015-1500-y.

Joshi S, Wang T, Araujo TLS, Sharma S, et al. (2018) Adapting to stress-chaperome networks in cancer. *Nat Rev Cancer* **18**: 562–575. https://doi.org/10.1038/s41568-018-0020-9.

Kim B, Kim D, Park J, Na H-K, Surh Y-J (2013) Ginsenoside Rg 3 induces apoptosis of human breast cancer (MDA-MB-231) cells. *J Cancer Prev* **18**: 177–185. https://doi.org/10.15430/jcp.2013.18.2.177.

Kordezangeneh M, Irani S, Mirfakhraie R, Esfandyari-Manesh M, Atyabi F, Dinarvand R (2015) Regulation of BAX/Bcl2 gene expression in breast cancer cells by docetaxel-loaded human serum albumin nanoparticles. *Med Oncol* **32**: 208. https://doi.org/10.1007/s12032-015-0652-5.

Korkola JE, DeVries S, Fridlyand J, Hwang ES, Estep AL et al. (2003) Differentiation of lobular versus ductal breast carcinomas

by expression microarray analysis. *Cancer Res* **63**: 7167–7175. Epub 2003/11/13. PMID:14612510.

Krajka-Kuźniak V, Paluszczak J, Baer-Dubowska W. (2017) The Nrf2-ARE signaling pathway: An update on its regulation and possible role in cancer prevention and treatment. *Pharmacol Rep* **69**: 393–402. https://doi.org/10.1016/j.pharep.2016.12.011.

Li Y, Chen Y, Qiu C, Ma X, Lei K, Gai G, Liang X, Liu J (2018) 17-Allylamino-17-demethoxygeldanamycin impeded chemotherapy through antioxidant activation *via* reducing reactive oxygen species-induced cell death. *J Cell Biochem* **120**: 1560–1576. https://doi.org/10.1002/jcb.27397.

Ling LU, Tan KB, Lin H, Chiu GNC (2011) The role of reactive oxygen species and autophagy in safingol-induced cell death. *Cell Death Dis* **2**: e129. https://doi.org/10.1038/cddis.2011.12.

López-Marure R, Contreras PG, Dillon JS (2011) Effects of dehydroepiandrosterone on proliferation, migration, and death of breast cancer cells. *Eur J Pharmacol* **660**: 268–2674. https://doi.org/10.1016/j.ejphar.2011.03.040.

Lu D-Y, Lu T-R, Cao S (2013) Drug combinations in cancer treatments. *Clin Experm Pharmacol* **2**: 6. https://doi.org/10.4172/2161-1459.1000134

Menon SS, Guruvayoorappan C, Sakthivel KM, Rasmi RR (2019) Ki-67 protein as a tumour proliferation marker. *Clin Chim Acta* **491**: 39–45. https://doi.org/10.1016/j.cca.2019.01.011.

Miller S, Stolze B, Fröhling S, et al. (2016) Prospective identification of resistance mechanisms to HSP90 inhibition in KRAS mutant cancer cells. *Oncotarget* **8**: 7678–7690. https://doi.org/10.18632/oncotarget.

Mitsuishi Y, Taguchi K, Kawatani Y, Kawatani Y, Shibata T, Nukiwa T, Aburatani H, Yamamoto M, Motohashi H (2012) Nrf2 Redirects glucose and glutamine into anabolic pathways in metabolic reprogramming. *Cancer Cell* **22**: 66–79. https://doi.org/10.1016/j.ccr.2012.05.016.

Nagashio R, Oikawa S, Yanagita K, Hagiuda D, Kuchitsu Y, et al. (2019) Prognostic significance of G6PD expression and localization in lung adenocarcinoma. *Biochim Biophys Acta – Proteins and Proteomic* **1867**: 38–46. https://doi.org/10.1016/j.bbapap.2018.05.005.

Nakai K, Xia W, Liao HW, Saito M, Hung M-C, et al. (2018) The role of PRMT1 in EGFR methylation and signaling in MDA-MB-468 triple-negative breast cancer cells. *Breast Cancer* **25**: 74–80. https://doi.org/10.1007/s12282-017-0790-z.

Nedeljković M, Damjanović A (2019) Mechanisms of chemotherapy resistance in triple-negative breast cancer – How we can rise to the challenge. *Cells* **8**: 957. https://doi.org/10.3390/cells8090957.

O'Loughlin M, Andreu X, Bianchi S, Chemielik E, Cordoba A (2018) Reproducibility and predictive value of scoring stromal tumour infiltrating lymphocytes in triple-negative breast cancer: a multi-institutional study. *Breast Cancer Res Treat* **171**: 1–9. https://doi.org/10.1007/s10549-018-4825-8.

Pareja F, Geyer FC, Marchiò C, Burke KA, Weigelt B, Reis-Filho J (2016) Triple-negative breast cancer: the importance of molecular and histologic subtyping and recognition of low-grade variants. *Npj Breast Cancer* **2**: 16036. https://doi.org/10.1038/npjbcancer

Pellegrino B, Musolino A, Llop-Guevara A, Serra V, De Silva P, Hlavata Z, Sangiolo D, Willard-Gallo K, Solinas C (2020) Homologous recombination repair deficiency and the immune response in breast cancer: A literature Review. *Transl Oncol* **13**: 410–422. https://doi.org/10.1016/j.tranon.2019.10.010.

Rahman NA, Yazan LS, Wibowo A, Ahmat N, Biau J, Tor YS, Yeap SK, Razali ZA, Ong YS, Fakurazi S (2016) Induction of apoptosis and G2/M arrest by ampelopsin E from Dryobalanops towards triple negative breast cancer cells, MDA-MB-231. *BMC Complement Altern Med* **16**: 354. https://doi.org/10.1186/s12906-016-1328-1.

Repetto G, del Peso A, Zurita JL (2008) Neutral red uptake assay for the estimation of cell viability/ cytotoxicity. *Nat Protoc* **3**: 1125–1131. https://doi.org/10.1038/nprot.2008.75.

Rouhi A, Miller C, Stolze B, Fröhling S, Reinhart S, Stolze B, Dohner H, Kuchenbauer F, Bullinger L, Frohling S, Scholl C (2017) Prospective identification of resistance mechanisms to HSP90 inhibition in KRAS mutant cancer cells. *Oncotarget* **8**: 7678–7690. https://doi.org/10.18632/oncotarget.13841.

Sami E, Paul BT, Koziol JA, Elshamy WM (2020) The immunosuppressive microenvironment in BRCA1-IRIS-overexpressing TNBC tumours is induced by bidirectional interaction with tumour associated macrophages. *Cancer Res* **80**: 1102–1117. https://doi.org/10.1158/0008-5472.CAN-19-2374.

Sidera K, Patsavoudi E (2014) HSP90 inhibitors: current development and potential in cancer therapy. *Recent Pat Anticancer Drug Discov* **9**: 1–20. https://doi.org/10.2174/15748928113089990031

Speranza G, Anderson L, Chen AP, Do K, Eugeni M (2018) First-in-human study of the epichaperome inhibitor PU-H71: clinical results and metabolic profile. *Invest New Drugs* **36**: 230–239. https://doi.org/10.1007/s10637-017-0495-3.

Su JC, Mar AC, Wu SH, et al. (2016) Disruptive VEGF – A paracrine and autocrine loops by targeting SHP-1 suppresses triple megative breast cancer metastasis. *Sci Rep* **6**: 28888. https://doi.org/10.1038/srep28888.

Sukhatme VP, Chan B (2012) Glycolytic cancer cells lacking 6-phosphogluconate dehydrogenase metabolize glucose to induce senescence. *FEBS Lett* **586**: 2389–2395. https://doi.org/10.1016/j.febslet.2012.05.052.

Trachootham D, Alexandre J, Huang P (2009) Targeting cancer cells by ROS-mediated mechanisms: a radical therapeutic approach? *Nat Rev Drug Discov* **8**: 579–591. https://doi.org/10.1038/nrd2803.

Trendowski M (2015) PU-H71: an improvement on nature's solutions to oncogenic Hsp90 addiction. *Pharmacol Res* **99**: 202–216. https://doi.org/10.1016/j.phrs.2015.06.007.

Turturro F, Friday E, Welbourne T (2007) Hyperglycemia regulates thioredoxin-ROS activity through induction of thioredoxin-interacting protein (TXNIP) in metastatic breast cancer-derived cells MDA-MB-231. *BMC Cancer*. **7**: 1–7. https://doi.org/10.1186/1471-2407-7-96.

Wang K, Jiang J, Lei Y, Zhou S, Wei Y, Huang C (2019) Targeting metabolic–redox circuits for cancer therapy. *Trends Biochem Sci* **44**: 401–414. https://doi.org/10.1016/j.tibs.2019.01.001.

Wang PG, Li YT, Pan Y, Gao Z-Z, Guan X-W, Jia L, Liu F-T (2019) Lower expression of Bax predicts poor clinical outcome in patients with glioma after curative resection and radiotherapy/chemotherapy. *J Neurooncol* **141**: 71–81. https://doi.org/10.1007/s11060-018-03031-9.

Wu J, Liu T, Rios Z, Mei Q, Lin X, Cao S (2017) Heat shock proteins and cancer. *Trends Pharmacol Sci* **38**: 226–256. https://doi.org/10.1016/j.tips.2016.11.009.

Yadav BS, Chanana P, Jhamb S (2015) Biomarkers in triple negative breast cancer: A review. *World J Clin Oncol* **6**: 252–263. https://doi.org/10.5306/wjco.v6.i6.252.